Applied Catalysis B: Environmental 181 (2016) 16–23

Contents lists available at ScienceDirect

Applied Catalysis B: Environmental

journal homepage: www.elsevier.com/locate/apcatb

A MoS_2/6,13-pentacenequinone composite catalyst for visible-light-induced hydrogen evolution in water

Yong-Jun Yuan[a], Zhen-Tao Yu[b,c,*], Yong-Hui Li[c], Hong-Wei Lu[a], Xin Chen[b,*], Wen-Guang Tu[c], Zhen-Guo Ji[a], Zhi-Gang Zou[c]

[a] College of Materials and Environmental Engineering, Hangzhou Dianzi University, Hangzhou, Zhejiang 310018, China
[b] National Laboratory for Infrared Physics, Shanghai Institute of Technical Physics, Chinese Academy of Sciences, Shanghai 200083, China
[c] Collaborative Innovation Center of Advanced Microstructures, College of Engineering and Applied Science, Nanjing University, and Kunshan Innovation Institute of Nanjing University, Nanjing, Jiangsu 210093, China

ARTICLE INFO

Article history:
Received 1 June 2015
Received in revised form 10 July 2015
Accepted 19 July 2015
Available online 26 July 2015

Keywords:
Hydrogen production
Molybdenum disulfide
Noble-metal-free
6,13-Pentacenequinone
Photocatalyst

ABSTRACT

6,13-Pentacenequinone (PQ) actively catalyzed the light-driven evolution of hydrogen in water when using MoS_2 nanosheets as cocatalyst. The MoS_2/PQ composite photocatalyst was prepared via a facile procedure and was fully characterized by X-ray diffraction (XRD), Raman spectroscopy, high-resolution transmission electron microscopy (HRTEM), X-ray photoelectron spectroscopy and UV–vis spectroscopy. Layered MoS_2 was incorporated on the PQ surface and served as electron traps. This allowed active sites to efficiently promote the separation of photogenerated carriers, thus facilitating the photocatalytic production of hydrogen from water. The effects of the MoS_2 loading on the PQ morphology and the pH of the reaction have been evaluated using triethanolamine (TEOA) as a sacrificial reductant. The photocatalytic results showed that the MoS_2/PQ composite photocatalyst manifested the highest H_2 production rate of 79.5 μmol h^{-1} g^{-1} under visible light irradiation ($\lambda > 420$ nm) at a MoS_2 concentration of 0.5 wt%, which exceeds the optimized photocatalytic H_2 evolution activity of Pt-loaded PQ (Pt/PQ) photocatalyst. The heterogeneous catalyst could be readily recovered and recycled at least three times without a significant loss of activity. This study provides new insights into solar-to-energy conversion using composite photocatalysts that are free of noble metals, are environmentally friendly and are responsive to visible light.

1. Introduction

Hydrogen production from photocatalytic water splitting has been the subject of intensive study because it offers a promising long-term approach for the utilization and conversion of solar energy into fuels [1]. To date, most of the research on fuel-forming reactions has been mainly focused on functionalized inorganic semiconductors, including oxides [2–7], sulfides [8,9], oxynitrides [10,11] and phosphates [12], used as photocatalysts [13–15], but only a few of them are considered to be suitable materials for effective photocatalysts that can operate the reactions efficiently with adequate lifetimes. With the goal of improving photoelectrochemical energy conversion, the development of modified well-known semiconductors such as TiO_2 as catalysts by metal loading [16], metal iondoping [17,18], or dye sensitization [19,20] is greatly needed. As an alternative, a new class of visible light-active solids could be sought out for this application [21]. Recently, several organic polymeric materials including poly(*p*-phenylene) [22], graphitic carbon nitride (g-C_3N_4) [23,24], polyimide [25], poly(azomethine) [26] and $C_3N_3S_3$-polymer [27] have been demonstrated to be active for water reduction, but most of these materials exhibited obviously lower values for their photocatalytic effectiveness than those of conditioned heterogeneous photocatalysts.

From the material design point of view, the band structure of organic solids can be directly tuned in these molecules by wise structural adjustment in the organic motifs associated with the charge transfer process, which is the key step in performing light-to-energy conversion. Organic molecular light-capturing materials have been widely used in both dye-sensitized solar cells [28] and homogeneous photocatalytic water reduction systems [29–31]. However, the possible application of simple organic molecular solids as photocatalysts for the light-driven generation

* Corresponding authors at: National Laboratory for Infrared Physics, Shanghai Institute of Technical Physics, Chinese Academy of Sciences, Shanghai 200083, China.
E-mail addresses: yuzt@nju.edu.cn (Z.-T. Yu), xinchen@mail.sitp.ac.cn (X. Chen).

http://dx.doi.org/10.1016/j.apcatb.2015.07.030
0926-3373/

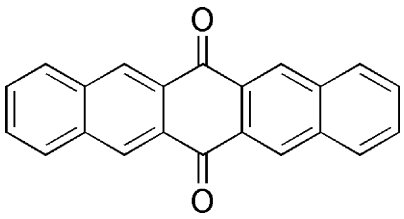

Scheme 1. Chemical structure of 6,13-pentacenequinone (PQ).

of hydrogen in a heterogeneous system has rarely been considered. Pentacenequinone derivatives are used as n-type organic semiconductors in organic thin film transistor devices due to their unique electronic properties [32]. A recent study has shown that 6,13-pentacenequinone (PQ) (Scheme 1) is photocatalytically active for H_2S splitting under visible light irradiation [33]. Compared with H_2S cleavage, the energy required to drive photocatalytic water splitting is much higher [34]. Therefore, the development of a new system based on PQ for the production of valuable fuels through the utilization of an extensive variety of water sources is of special importance.

It has been demonstrated that the deposition of suitable cocatalysts on the catalyst particles exerts an impressive impact on upgrading the effectiveness of catalysts for the generation of hydrogen from water [16]. Currently, precious metal species such as Pt are widely considered as effective co-catalysts in promoting the evolution of hydrogen [35]. The catalytic performance of the cocatalysts in such a photocatalytic system strongly depends on their chemical and physical characteristics such as particle size, dispersibility, contact with photocatalysts, valence states and so on. For widespread application, the utilization of non-noble metal alternatives with high efficiencies and low costs is particularly attractive. Recently, graphene-like molybdenum disulfide (MoS_2) has proven to be an impressive and appealing catalyst for electrochemical hydrogen evolution reaction [36–39], most likely due to the presence of the exposed active edge sites that offer highly accessible reactive sites [40]. Layered MoS_2 alone is not generally a viable photocatalyst for hydrogen production in the absence of any other semiconductor or photosensitizer [41], despite the fact that it absorbs very effectively at visible wavelengths, which is likely because of insufficient charge separation. Several promising examples of photocatalytic hydrogen evolution [42–45] and organic dye degradation [46,47] using MoS_2 as an efficient cocatalyst have appeared, but the effect of a cocatalyst based on MoS_2 on the catalytic performance remains less understood. Herein, we first demonstrate that PQ can effectively catalyze hydrogen production from water with the help of a MoS_2 nanoparticle cocatalyst under visible light irradiation. Moreover, our results show that MoS_2 has a good performance as a cocatalyst that exceeds that of Pt metal for photocatalytic hydrogen production under visible light irradiation. This study presents a new inorganic–organic photocatalytic composite material for solar-to-hydrogen conversion.

2. Experimental

2.1. Chemicals

All of the chemical reagents were used as supplied without further purification. For cyclic voltammetry measurements, anhydrous acetonitrile was supplied by Alfa Aesar, and tetrabutylammonium hexafluorophosphate was obtained from Sigma Aldrich.

2.2. Instrumentation

^{1}H NMR spectra were measured on a Bruker AMX500 MHZ FT NMR spectrometer. Analyses for C, H and N were performed on a Perkin-Elmer 240C element analyzer. UV–vis diffuse-reflectance spectroscopy experiments were performed with a Varian Cary 50 UV–vis spectrophotometer, and $BaSO_4$ was used as a reference standard. The photoluminescence emission spectra and luminescence lifetimes were measured at room temperature on a fluorescence spectrophotometer (Horiba Jobin-Yvon Fluorolog-3-21-TCSPC). Electrochemical properties were measured with a PARSTAT-2273 advanced electrochemical system. The nitrogen adsorption–desorption isotherm was obtained by nitrogen physisorption at 77 K on a surface area and porosity analyzer (Micromeritics TriStar, USA), and the surface area was calculated by the BET method. Thermogravimetric analysis (TGA) was achieved on a NETZSCH STA 449F3 thermal analysis system with a heating rate of 5 °C min^{-1}. The nanoscale images of PQ were obtained using a JEOL JEM-200CX transmission electron microscope or a NOVA NANOSEM230 scanning electron microscope. The Fourier transform infrared (FT-IR) spectra were recorded on a Nicolet-Nexus 870 infrared spectrophotometer by using the KBr pellet technique. The X-ray diffraction (XRD) profiles were obtained on a D/MAX-2500 automatic powder diffractometer equipped with graphite monochromatized Cu Kα radiation (λ = 0.1542 nm) flux at a scanning rate of 5° min^{-1} in the 2θ range of 10–80°. The Raman spectra of samples were acquired on a Renishaw Raman microscope spectrometer (RM-1000, Great Britain) under 785 nm diode laser excitation. The X-ray photoelectron spectra (XPS) were acquired on a Kratos Axis Ultra DLD spectrometer using a monochromatic Al Kα radiation.

2.3. Preparation and characterization

2.3.1. 6,13-Pentacenequinone

PQ was synthesized by a modified method according to a previously reported procedure [33]. In a 100 mL reaction flask, *o*-phthaldialdehyde (2.68 g, 20 mmol) and 1,4-cyclohexanedione (1.12 g, 10 mmol) were dispersed in 15 mL of water by ultrasound. A 15-mL aliquot of KOH (15 wt%) solution was added to the mixture with continuous magnetic stirring to induce the precipitation of a yellow solid. The solid product was then filtered out, washed by water (3× 20 mL) and washed by acetone (3× 20 mL) to remove the unreacted reactants (yield: 62%). ^{1}H NMR (500 MHz, $CDCl_3$, δ): 8.99 (4H, s), 8.18 (4H, d, J = 7.5), 7.73 (4H, t, J = 8). IR (KBr): ν = 3051, 1673, 1612, 1563, 1445, 1394, 1277, 1187, 991, 762, 540, 475. Anal. calcd. for $C_{22}H_{12}O_2$: C 73.36, H 3.83; found: C 73.47, H 3.96.

2.3.2. MoS_2/PQ

The MoS_2/PQ composites were prepared via a two-step procedure. First, the nano-structured MoS_2 was prepared by a reported hydrothermal reaction of sodium molybdate dehydrate and thiourea [7]. Secondly, the MoS_2/PQ composites loaded with various amounts of MoS_2 were prepared in a similar method. In a typical synthesis of the 0.5 wt% MoS_2/PQ composite, 0.50 mg of MoS_2 was dispersed under magnetic stirring in 50 mL of aqueous solution containing 100 mg of PQ, and then the mixture was shaken in an ultrasonic bath for 1 h to form a suspension. The resulting mixture was centrifuged, and the separated solid was rinsed with water followed by drying at 80 °C overnight. Finally, the sample was heat-treated at 300 °C under a nitrogen atmosphere for 4 h.

2.4. Electrochemical studies

Cyclic voltammetry (CV) was recorded under a nitrogen atmosphere with a scan rate of 50 mV s^{-1} using a three-electrode system

consisting of Ag/AgCl as the reference electrode, a platinum sheet as the counter electrode, and a glassy carbon disk as the working electrode. The supporting electrode was 0.1 M tetrabutylammonium hexafluorophosphate (Bu_4NPF_6) in acetonitrile. The *J–V* curve was recorded on a CHI-B600 electrochemical analyzer, and the light source was a 300 W Xe lamp. Photoelectrochemical experiment was performed using a three-electrode cell configuration of the photo-anode (working electrode), Pt sheet (counter electrode) and Ag/AgCl electrode (reference electrode) in a 0.5 M Na_2SO_4 solution. The photoanodes of PQ or other composite samples were prepared by spin coating a saturated dichloromethane solution of PQ or MoS_2/PQ (1 mg mL^{-1}) on ITO glass, which was then heated at 300 °C for 4 h.

2.5. Photocatalytic H_2 production

Photocatalytic hydrogen evolution reactions were carried out at room temperature in a Pyrex vessel, which was connected to a glass closed gas circulation and evacuation system. The experiment was performed by dispersing MoS_2/PQ powder (100 mg) in an aqueous solution (100 mL) containing triethanolamine (0.2 M) as a sacrificial electron donor. The pH value of the solution was adjusted by the addition of 38 wt% hydrochloric acid. The reaction solution was evacuated several times to completely remove any air. After evacuation, the mixture was exposed to visible irradiation ($\lambda > 420$ nm) using a Xenon lamp (300 W equipped with a cut-off filter) with gentle magnetic stirring. The gases being evolved were periodically detected in situ on a gas chromatograph equipped with a thermal conductivity detector (Shimadzu GC-8A, argon as the carrier gas and a MS-5A column).

2.6. DFT calculations

The density functional theory calculations (B3LYP/LANL2DZ) for PQ were performed using *Gaussian 09* package [48]. The numerical calculations in this paper were performed on the IBM Blade cluster system at the High Performance Computing Center (HPCC) of Nanjing University.

3. Results and discussion

3.1. Preparation and properties of the catalyst

The MoS_2/PQ composite photocatalyst was obtained via an easy two-step method (see Section 2). PQ was first synthesized by a method modified from a previously reported procedure and was full characterized by ^{1}H NMR, XRD, FT-IR and elemental analysis. The sample seems to be insoluble in water but soluble in polar organic solvents such as dichloromethane, acetonitrile and acetone. The structure of PQ powder was investigated by powder X-ray diffraction (XRD). The scanning electron microscope (SEM) image of PQ particles shows that the square-shaped particles are closely packed together in the solid (Fig. S1, see Supporting information). The Brunauer–Emmett–Teller (BET) specific surface area of PQ was determined to be approximately 10.6 m^2 g^{-1} (Fig. S2). Thermogravimetric analysis revealed that PQ is thermally stable up to approximately 360 °C (Fig. S3). The strong intermolecular π–π stacking interactions in PQ may impart this good thermal stability. The photophysical properties and redox behavior of PQ are in very good agreement with the published data [33]. As indicated by the yellow color of PQ, an optical absorption edge in the range of visible light is observed in a CH_2Cl_2 solution (Fig. S4), which is associated with the transition from the highest occupied molecular orbital to the lowest unoccupied molecular orbital (HOMO-LUMO) (Fig. S5). Based on density functional theory (DFT) calculations, the HOMO is localized mainly on the aromatic ring moiety, while the LUMO corresponds to a mixture of the dione moiety with a minor contribution from the aromatic ring moiety. The electronic redistribution clearly implies that a significant intramolecular charge separation between the HOMO and LUMO levels could easily occur. Under the illumination of visible light ($\lambda > 420$ nm, 300 W), the PQ layer coated on indium tin oxide (ITO) glass plates can generate a photocurrent of ca. 2 μA/cm^2 in a 0.50 M Na_2SO_4 aqueous solution (Fig. S6), indicating that an efficient separation of the photogenerated charge carriers occurred. This value is close to that of bulk g-C_3N_4 [49].

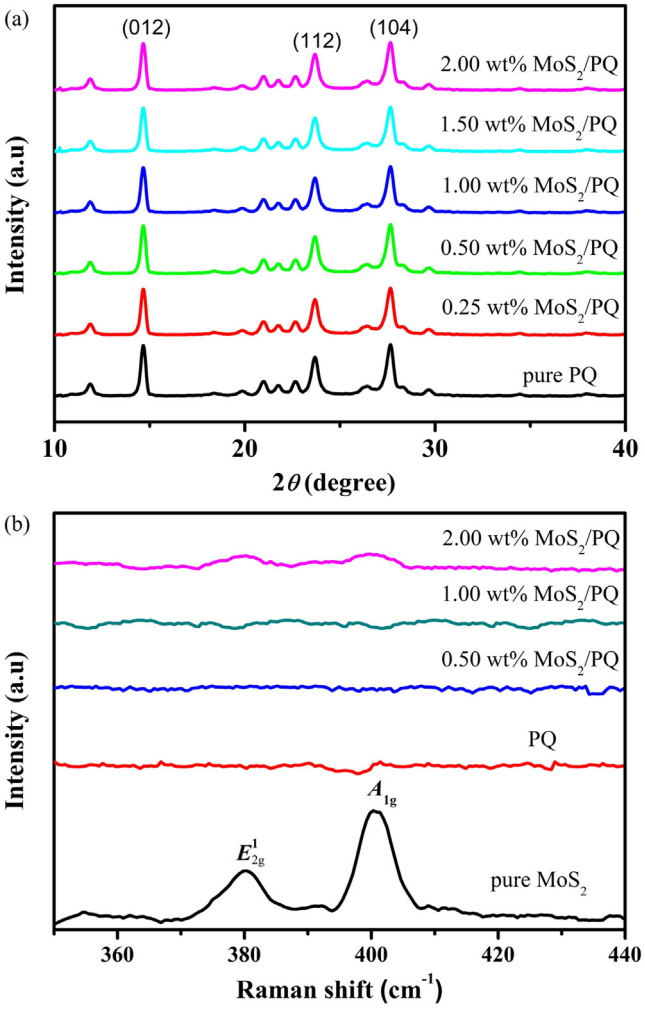

Fig. 1. (a) XRD patterns and (b) Raman spectra of PQ and MoS_2/PQ composites as a function of the MoS_2 loading used during the preparation.

The MoS_2 nanosheets, as the other precursor for the fabrication of the MoS_2/PQ composite photocatalyst, were obtained from a reported hydrothermal method [7]. The MoS_2/PQ composite photocatalyst was made via the ultrasonic dispersion of nanocrystalline powders of MoS_2 in water with the addition of PQ, followed by sintering up to 300 °C under a nitrogen atmosphere.

As shown in Fig. 1, the XRD spectrum of PQ power displays main diffraction peaks at $2\theta = 14.6°$, 23.6° and 27.6°. Referring to the literature, these peaks correspond to the reflections from the (0 1 2), (1 1 2) and (1 0 4) planes (JCPDS, 47-2123) [50], respectively. The good crystalline quality of the sample was confirmed by the sharpness and high intensities of the diffraction peaks. As for the pure nanostructured MoS_2 particles, the XRD pattern of the pure and poorly crystallized MoS_2 reveals distinct characteristic peaks at 14.0°, 33.5°, 38.8° and 58.1° corresponding to diffraction from the (0 0 2), (1 0 0), (1 0 3) and (1 1 0) lattice planes of the hexagonal MoS_2 phase (JCPDS card no: 87-2416, molybdenum disulfide 2H)

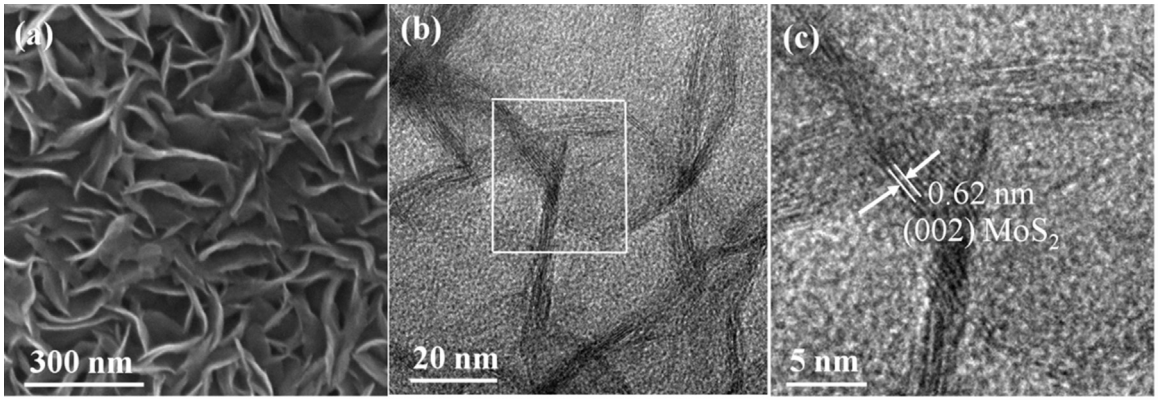

Fig. 2. (a) SEM image of pure MoS_2, (b) HRTEM image of the 2.0 wt% MoS_2/PQ composite, and (c) the magnified HRTEM image of a selected frame from image (b).

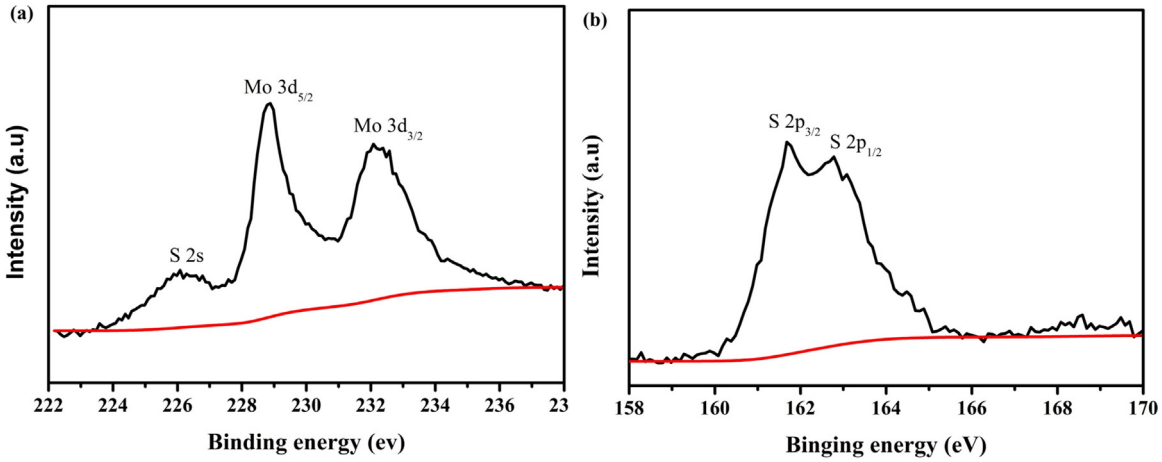

Fig. 3. XPS spectra of the 2.0 wt% MoS_2/PQ photocatalyst.

[42], as shown in Fig. S7. However, no diffraction peaks attributed to the MoS_2 species were observed in the XRD spectrum of the MoS_2/PQ composite due to the small MoS_2 content and its high dispersion on the surface of PQ that existed in the MoS_2/PQ composites. Similar behaviors were also observed in other MoS_2-based composites [45]. Meanwhile, Raman spectra of pure MoS_2 and MoS_2/PQ composites were investigated to confirm the maintained 2H-MoS_2 structure after coating the PQ surfaces with MoS_2. As shown in Fig. 1(b), the pure MoS_2 nanosheets show two typical peaks at 382 and 401 cm^{-1}, which can be assigned to the in-plane $E^1{}_{2g}$ vibration and the out-of-plane A_{1g} vibration of the hexagonal MoS_2, respectively. For the MoS_2/PQ composites, no peaks of MoS_2 can be seen in the Raman spectra of both the 0.50 and 1.00 wt% MoS_2/PQ composites. For the 2.00 wt% MoS_2/PQ composite, the presence of weaker and broader E_{2g} and A_{1g} characteristic peaks indicates that the layered MoS_2 was coated on the surface of PQ. Further composition analysis using high-resolution transmission electron microscopy (HRTEM) combined with X-ray photoelectron spectroscopy (XPS) revealed the presence of MoS_2 in the MoS_2/PQ composites. A HRTEM image of the 2.0 wt% MoS_2/PQ composite illustrates that MoS_2 with its typical layered structure (Fig. 2), in which the lattice spacing is approximately 0.61 nm corresponding to the (0 0 2) plane of hexagonal MoS_2 [51,52], is deposited on the surface of PQ. An intimate interface between MoS_2 and PQ formed in the composites, which may provide a beneficial effect on the charge transfer between MoS_2 and PQ. From the high resolution XPS spectra of the 2.0 wt% MoS_2/PQ composite shown in Fig. 3, two peaks are present at 228.8 eV ($3d_{5/2}$) and 232.3 eV ($3d_{3/2}$) for Mo, and two peaks at 162.2 eV ($2p_{3/2}$) and 163.3 eV ($2p_{1/2}$) are also present in the S 2P region. This indicates that Mo and S are present in Mo^{4+} and S^{2-} valence states [52].

Fig. 4 shows a comparison of the UV–vis diffuse reflectance spectra of samples of PQ and MoS_2/PQ composites with different MoS_2 contents. The PQ shows semiconductor-like band gap absorption at 455 nm, corresponding to an optical bandgap of 2.76 eV. Loading PQ with MoS_2 imparts a distinct red shift and an increase of the

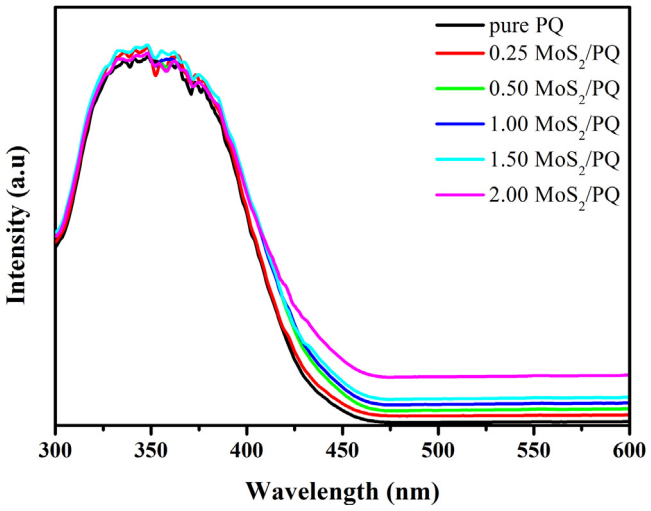

Fig. 4. UV–vis diffuse reflectance spectra of PQ and MoS_2/PQ composites.

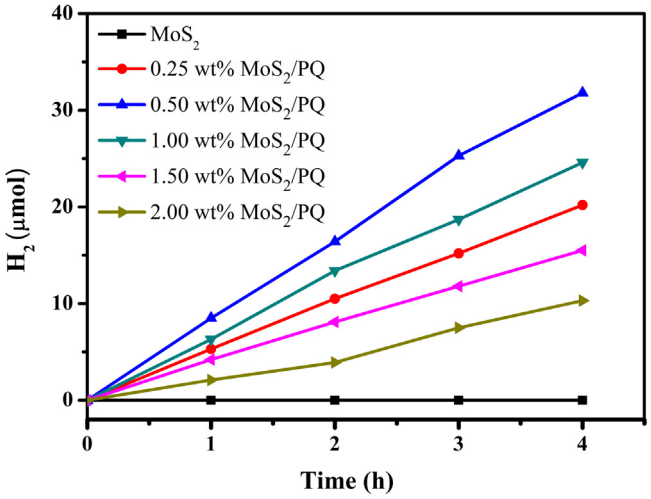

Fig. 5. Photocatalytic H_2 production activities over PQ loaded with different amounts of MoS_2 under visible light irradiation ($\lambda > 420$ nm) in a mixed aqueous solution containing 0.1 g of photocatalyst and 0.2 M TEOA at a pH of 7.0.

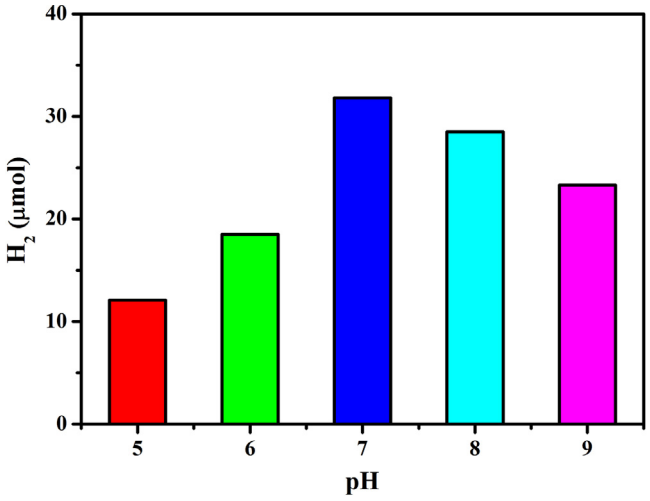

Fig. 6. Effect of the pH on the photogeneration of hydrogen for PQ loaded with 0.5 wt% MoS_2 under visible light irradiation ($\lambda > 420$ nm) in 100 mL of 0.2 M TEOA aqueous solution.

absorption band in the visible light region, which depicts a good interaction between MoS_2 and PQ. Additionally, it clearly shows that the light-harvesting ability of the composite strengthens with increasing amounts of MoS_2, which is also consistent with the fact that the color of the samples changed from yellow to gray.

3.2. Photocatalytic H_2 evolution activity

We then evaluated the photocatalytic activity of PQ in the context of hydrogen production. The studies were carried out in 100 mL of aqueous solution using TEOA as an electron donor under the illumination of visible light ($\lambda > 420$ nm). However, although PQ could absorb visible light, no H_2 evolution was detected under these conditions. After the MoS_2 nanosheets were loaded as H_2 evolution sites on the PQ surface, the formation of hydrogen was clearly observed. The control experiment showed that no hydrogen evolution was obtained in the dark, indicating that the evolution of H_2 is initiated by light. Based on these results, it is reasonable to conclude that the MoS_2-loaded PQ composite (MoS_2/PQ) has the capacity to catalyze the reduction of water under visible light.

Fig. 5 shows a plot of the variation in the photocatalytic H_2 evolution activities of PQ samples loaded with different amounts of MoS_2 cocatalyst, and it indicates that the photocatalytic performance of PQ is greatly influenced by the MoS_2 loading amount. These results showed that the rate of hydrogen evolution initially increased with increasing MoS_2 content, reached a maximum at 0.5 wt% MoS_2 and then decreased upon a further increase in the MoS_2 loading amount. This result consisted with the observation in photoelectrochemical response of the MoS_2/PQ composite photoelectrodes (Fig. S8). With a low loading amount of 0.25 wt% MoS_2, the photocatalyst showed a H_2 evolution rate of 50.5 $\mu mol\ h^{-1}\ g^{-1}$. When the loading amount of MoS_2 was increased to 0.5 wt%, the H_2 evolution rate was observed to be 79.5 $\mu mol\ h^{-1}\ g^{-1}$. With the enhancement of the MoS_2 loading amount to 2.0 wt%, the H_2 evolution rate decreased to 25.8 $\mu mol\ h^{-1}\ g^{-1}$. When the loading amount of MoS_2 is less than 0.5 wt%, the photocatalytic activity of the MoS_2/PQ composite photocatalyst increased with increasing MoS_2 loading amounts, which can be attributed to the increasing number of active catalytic sites on the MoS_2 for the water reduction reaction. However, a further increase in the MoS_2 loading amount to 1.5 or 2.0 wt% resulted in a decreased hydrogen evolution rate compared to the rate at a loading of 0.25 wt%. With increasing amounts of MoS_2, the color of the composite photocatalyst changed from yellow to gray. The introduction of a large amount of the black MoS_2 nanosheets on the surface of the PQ shielded the incident light from irradiating into the inside of the PQ light absorber, resulting in a decreased H_2 evolution rate. A similar observation has been encountered in previous studies [51,53].

When the pure unmodified MoS_2 nanosheets were used alone as a photocatalyst under identical experimental conditions, there was no appreciable hydrogen evolved under visible light irradiation, which is probably related to the surface properties of the catalyst. This observation is consistent with those previously reported in the study of the photocatalytic properties of MoS_2 [45]. We noted the MoS_2/PQ composite photocatalyst shows a lower photocatalytic activity than those of inorganic/inorganic composite photocatalysts such as MoS_2/TiO_2 (1.6 $mmol\ h^{-1}\ g^{-1}$) [52] or MoS_2/CdS (5.4 $mmol\ h^{-1}\ g^{-1}$) [8], but its activity is comparable to those of inorganic/organic composite photocatalysts such as MoS_2/C_3N_4 (17.8 $\mu mol\ h^{-1}\ g^{-1}$) [45]. For inorganic compound-based composite photocatalysts, an intimate interface between the two components in the heterostructures facilitates the charge transfer and thus restrains their recombination by coupling two well-matched overlapping semiconductor band structures, leading to the enhancement of photocatalytic H_2 production activity. Whereas, it is difficult to create effective interfacial contacts between PQ and MoS_2 due to the different physical characteristics of resilient organic and hard inorganic compounds, leading to the lower photocatalytic activity of the MoS_2/PQ composite photocatalyst relative to related inorganic composite photocatalysts.

To further optimize the performance of the MoS_2/PQ photocatalyst, the effects of the pH value on the photocatalytic hydrogen evolution activity were also investigated using 0.5 wt% MoS_2/PQ photocatalyst (Fig. 6). The rate of light-induced H_2 evolution was found to depend on the pH value when it was varied from 5.0 to 9.0. A maximum rate of H_2 production was observed at a pH of 7.0, and lower rates were obtained when either lower or higher pH values were used. The decrease in the rate of H_2 evolution at higher pH values is likely a result of a lower proton concentration in the reaction solution; moreover, when the pH value of the bulk solution is increased, the thermodynamic driving force for proton reduction is lower. Conversely, lowering the pH value from 7.0 to 5.0 leads to the protonation of TEOA, which is an ineffective sacrificial electron donor. The maximal H_2 generation rate was observed at a neutral pH. This phenomenon could be attributed to a balance between the benefit of the higher proton concentration at a low pH value and

Table 1
Photocatalytic H_2 evolution activities of PQ loaded with different amounts of Pt cocatalyst.[a]

Entry	Pt (wt%)[b]	H_2 evolution rate (μmol h^{-1} g^{-1})
1	0.5	11.9
2	1.0	26.3
3	2.0	41.5
4	3.0	53.2
5	4.0	38.9
6	5.0	27.9

[a] Reaction conditions: photocatalyst, 100 mg; reaction solution, 100 mL of 0.2 M TEOA aqueous solution (pH 7.0); light source, 300 W Xe lamp with cutoff filter ($\lambda > 420$ nm).
[b] Pt cocatalysts were loaded by a photodeposition method in situ using K_2PtCl_4.

the need for TEOA as an electron donor for PQ regeneration at a high pH value.

To promote charge separation and extract the photogenerated electrons, the noble metal Pt cocatalyst has often been used in such a reductive reaction due to its large work function and relatively low overpotential for catalyzing the desired reaction at the desired rate [6,23]. For comparison, Pt cocatalyst was used instead of MoS_2 under our experimental conditions. When using K_2PtCl_4 as a precursor, the Pt nanoparticles (NPs) were loaded as H_2 evolution sites in situ on the PQ surface by the photodeposition method, which clearly resulted in the observable formation of hydrogen. As shown in Table 1, the H_2 evolution activity of PQ was also dependent on the Pt cocatalyst loading amount. The highest H_2 evolution rate of 53.2 μmol h^{-1} g^{-1} was obtained with 3.0 wt% Pt/PQ composite photocatalyst. Furthermore, the particle size of the Pt NPs deposited on the PQ was confirmed by TEM after 24 h of irradiation. A typical TEM image of the Pt NPs is shown in Fig. S9, which shows a fine dispersion of approximately 3- to 5-nm-diameter Pt NPs on the surface of PQ. The observed size of the Pt NPs makes them applicable for use as a cocatalyst in photocatalytic H_2 generation [54]. The results indicate that MoS_2 is more effective as a cocatalyst than Pt under the reaction conditions, which may be related to the effective intimate surface formed between MoS_2 and PQ, as shown by the HRTEM image.

The stability of the H_2 evolution system was also examined by operating the photoinduced H_2 evolution experiment three consecutive times under the same reaction conditions. As shown in Fig. 7, the amounts of H_2 produced in the photocatalytic system based on a 0.5 wt% MoS_2-loaded PQ sample increased steadily

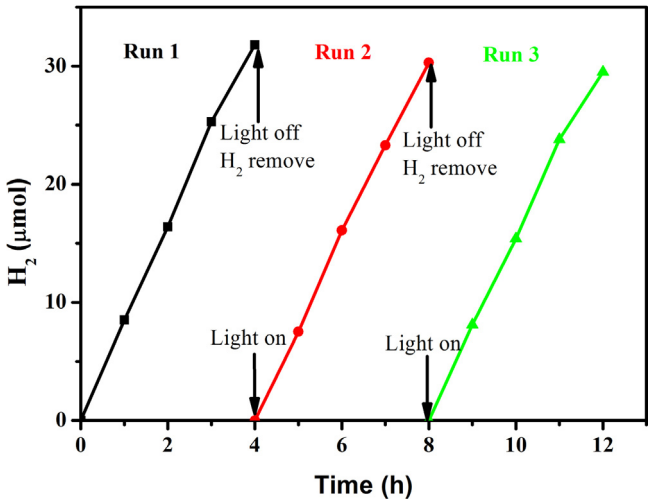

Fig. 7. Recycling H_2 evolution test for PQ loaded with 0.50 wt% MoS_2 under visible light irradiation ($\lambda > 420$ nm) in 100 mL of 0.2 M TEOA aqueous solution at a pH of 7.0.

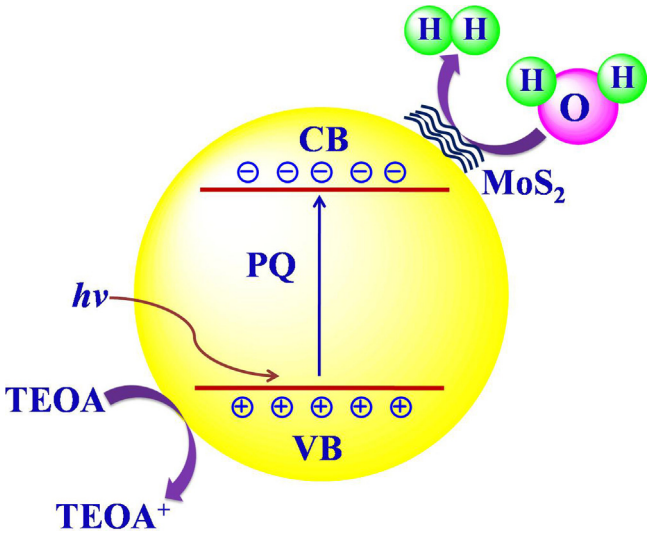

Fig. 8. Schematic diagram of proposed mechanisms of visible-light-induced hydrogen production over the MoS_2/PQ composite catalyst.

with a prolonged light irradiation time. The catalyst was reused for the three successive trials for a cumulative time of 12 h without a considerable decrease in the efficiency of the catalyst. A similar stability study was carried on a 3.0 wt% Pt-loaded PQ sample, as shown in Fig. S10. It is worth noting that no obvious change in the material structure was observed for PQ after 72 h of irradiation, which was confirmed by the XRD and FTIR examinations (Figs. S11 and S12). Therefore, the photochemical stability of PQ is acceptable for light-induced hydrogen evolution.

3.3. Mechanism of photocatalytic hydrogen production

The exact reaction process still remains highly uncertain, and the possible mechanisms for the reaction are illustrated in Fig. 8. The photocatalytic hydrogen evolution reaction with MoS_2 as a cocatalyst may favor proceeding via a Volmer-Heyrovsky pathway as discussed in a previous report [55–57]. Upon excitation, an excited PQ molecule is created. Such an excited state as a strong reduction potential, which can be estimated by spectroscopic and electrochemical investigations (Figs. S13 and S14). The value of the excited state oxidation potential (E_{ox}^*) of PQ (−0.83 V vs. NHE) is more negative than the redox potential of protons [$E(H^+/H_2) = -0.41$ V vs. NHE at a pH 7], which suggests that there would be enough driving force for the reduction of protons to yield H_2 (Fig. S15). However, the reduction of water with the evolution of hydrogen failed to occur when using PQ alone, which was most likely because of both the fast recombination of the photogenerated electron–hole pairs in PQ and the high overpotential of the water reduction reaction [16]. MoS_2 has a suitable redox potential, which is less negative than the H^+/H_2 potential and more positive than the CB of PQ [7], allowing it to be exploited as an efficient cocatalyst to facilitate an efficient water-splitting chemical reaction. In the meantime, the high H_2 activation capability of MoS_2 has been verified to be beneficial for hydrogen production [39]. After loading MoS_2 on the PQ surface, the photogenerated electrons were transferred from the excited state PQ to MoS_2, where the electrons subsequently combine with the adsorbed H^+ ions in water to yield H_2. In the process, the MoS_2 cocatalyst acts as photocatalytic reaction centers leading to efficient interfacial charge transfer [7]. This efficient charge transfer prevents recombination and thus is responsible for the unique H_2 production activity of MoS_2/PQ composite photocatalysts.

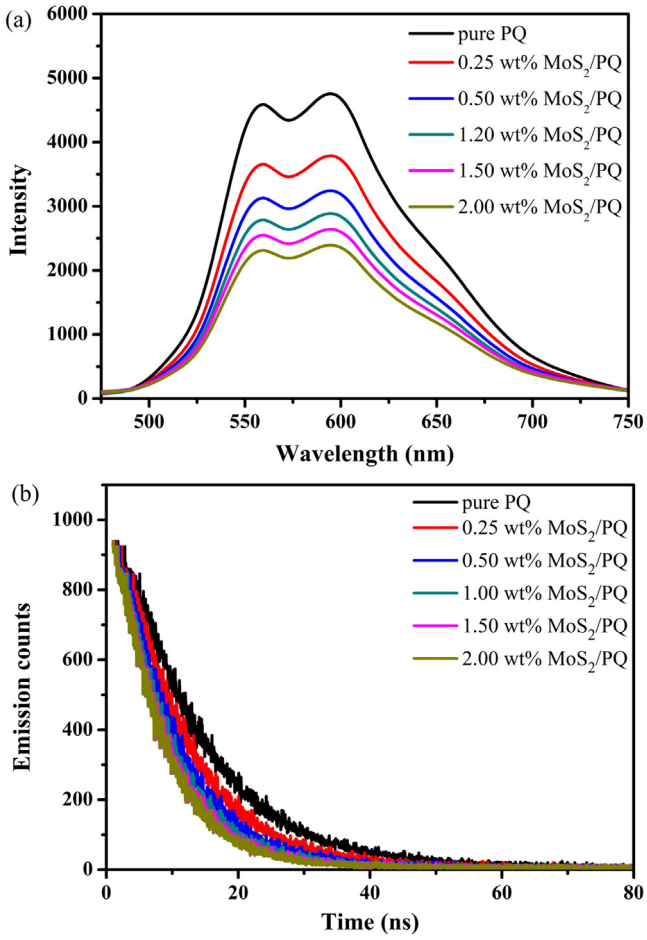

Fig. 9. Comparison of photoluminescence spectra (a) and decay curves (b) of PQ and MoS_2/PQ composites.

To investigate the photo-induced electron transfer between composites, the steady-state and time-resolved luminescence spectra of PQ in the absence and presence of MoS_2 were measured. As shown in Fig. 9, photoluminescence spectra reveal that the as-prepared neat PQ and all of the MoS_2/PQ composite catalysts show only one type of luminescence peaks in the recorded spectra, and the luminescence quenching of PQ takes place in the presence of MoS_2 at an excitation wavelength of 350 nm. The luminescence intensity decreased with an increase in the amount of MoS_2, indicating that the unwanted charge recombination process can be suppressed by the presence of MoS_2. In addition, neat PQ has an excited state lifetime of 16 ns at room temperature, and the lifetime of PQ is quenched resulting in a shorter lifetime when the MoS_2 was loaded onto the surface of PQ. From the luminescence decay curves, it is evident that the excited electrons from PQ have been readily transferred to the MoS_2 cocatalyst, thus effectively enhancing the separation efficiency of photogenerated electron/hole pairs. The lowest luminescence intensity and the shortest lifetime of the 2.0 wt% MoS_2-loaded PQ sample indicated that the recombination of charge carriers was minimized, but it did not show the best photocatalytic activity. The reason behind this finding has been discussed before. Such an improvement in the separation efficiency should contribute to an improved photocatalytic activity [51]. Therefore, this new type of MoS_2/PQ composite catalyst shows potential as a novel functional inorganic/organic hybrid material for photocatalytic hydrogen evolution from water and indicates that inorganic/organic hybrid materials offer promising strategies to obtain artificial materials with these promising properties.

4. Conclusions

In this contribution, the light-driven water reduction of PQ has been achieved with the aid of a MoS_2 cocatalyst and TEOA as a sacrificial electron donor under visible light irradiation. The MoS_2 loading amount significantly affected the photocatalytic behavior of the MoS_2/PQ composite catalysts. The PQ sample with a loading of 0.5 wt% MoS_2 afforded the best catalytic performance and allowed for a H_2 generation rate of 79.5 $\mu mol\ h^{-1}\ g^{-1}$ at a pH of 7.0 with good stability. Moreover, MoS_2 appears to be more effective than Pt as a cocatalyst when loaded on PQ for hydrogen production. The results represent a potential and prospective application of molecular organic materials for energy conversion and will generate interest in the development of more efficient and stable organic solids for storing solar energy in the form of chemical fuels.

Acknowledgments

This work was financially supported by the National Basic Research Program of China (Grant No. 2013CB632400), the Natural Science Foundation of Jiangsu Province (Grant No. BK20141233). Y.Y.J. acknowledges financial support from the School Science Starting Foundation of Hangzhou Dianzi University (Grant No. KYS205614038). We are also grateful to the Scientific Research Foundation for the Returned Overseas Chinese Scholars, State Education Ministry. We are grateful to the High Performance Computing Center (HPCC) of Nanjing University for doing the numerical calculations in this paper on its IBM Blade cluster system.

Appendix A. Supplementary data

Supplementary material related to this article can be found, in the online version, at http://dx.doi.org/10.1016/j.apcatb.2015.07.030

References

[1] A. Kudo, Y. Miseki, Chem. Soc. Rev. 38 (2009) 253–278.
[2] S. Kakuta, T. Abe, ACS Appl. Mater. Interfaces 1 (2009) 2707–2710.
[3] K. Maeda, Chem. Commun. 49 (2013) 8404–8406.
[4] X. Xu, C. Randorn, P. Efstathiou, J.T.S. Irvine, Nat. Mater. 11 (2012) 595–598.
[5] X. Wang, Q. Xu, M. Li, S. Shen, X. Wang, Y. Wang, Z. Feng, J. Shi, H. Han, C. Li, Angew. Chem. Int. Ed. 51 (2012) 13089–13092.
[6] J. Yu, L. Qi, M. Jaroniec, J. Phys. Chem. C 114 (2010) 13118–13125.
[7] Q. Xiang, J. Yu, M. Jaroniec, J. Am. Chem. Soc. 134 (2012) 6575–6578.
[8] X. Zong, H. Yan, G. Wu, G. Ma, F. Wen, L. Wang, C. Li, J. Am. Chem. Soc. 130 (2008) 7176–7177.
[9] Y.P. Xie, Z.B. Yu, G. Liu, X.L. Ma, H.M. Cheng, Energy Environ. Sci. 7 (2014) 1895–1901.
[10] K. Maeda, K. Domen, J. Phys. Chem. C 111 (2007) 7851–7861.
[11] K. Maeda, D. Lu, K. Domen, Chem. Eur. J. 19 (2013) 4986–4991.
[12] Z. Yi, J. Ye, N. Kikugawa, T. Kako, S. Ouyang, H. Stuart-Williams, H. Yang, J. Cao, W. Luo, Z. Li, Y. Liu, R.L. Withers, Nat. Mater. 9 (2010) 559–564.
[13] P. Ritterskamp, A. Kuklya, M.A. Wüstkamp, K. Kerpen, C. Weidenthaler, M. Demuth, Angew. Chem. Int. Ed. 46 (2007) 7770–7774.
[14] Z. Han, F. Qiu, R. Eisenberg, P.L. Holland, T.D. Krauss, Science 338 (2012) 1321–1324.
[15] Z.J. Li, J.J. Wang, X.B. Li, X.B. Fan, Q.Y. Meng, K. Feng, B. Chen, C.H. Tung, L.Z. Wu, Adv. Mater. 25 (2013) 6613–6618.
[16] J. Yang, D. Wang, H. Han, C. Li, Acc. Chem. Res. 46 (2013) 1900–1909.
[17] G. Liu, H.G. Yang, X. Wang, L. Cheng, J. Pan, G.Q. Lu, H.M. Cheng, J. Am. Chem. Soc. 131 (2009) 12868–12869.
[18] S. In, A. Orlov, R. Berg, F. García, S. Pedrosa-Jimenez, M.S. Tikhov, D.S. Wright, R.M. Lambert, J. Am. Chem. Soc. 129 (2007) 13790–13791.
[19] T. Kamegawa, S. Matsuura, H. Seto, H. Yamashita, Angew. Chem. Int. Ed. 52 (2013) 916–919.
[20] Y.J. Yuan, Z.T. Yu, X.Y. Chen, J.Y. Zhang, Z.G. Zou, Chem. Eur. J. 17 (2011) 12891–12895.
[21] G. Liu, P. Niu, L. Yin, H.M. Cheng, J. Am. Chem. Soc. 134 (2012) 9070–9073.
[22] S. Yanagida, A. Kabumoto, K. Mizumoto, C. Pac, K. Yoshino, J. Chem. Soc. Chem. Commun. (1985) 474–475.
[23] X. Wang, K. Maeda, A. Thomas, K. Takanabe, G. Xin, J.M. Carlsson, K. Domen, M. Antonietti, Nat. Mater. 8 (2009) 76–80.
[24] Z. Lin, X. Wang, Angew. Chem. Int. Ed. 52 (2013) 1735–1738.

[25] S. Chu, Y. Wang, Y. Guo, J. Feng, C. Wang, W. Luo, X. Fan, Z. Zou, ACS Catal. 3 (2013) 912–919.
[26] M.G. Schwab, M. Hamburger, X. Feng, J. Shu, H.W. Spiess, X. Wang, M. Antonietti, K. Müllen, Chem. Commun. 46 (2010) 8932–8934.
[27] Z. Zhang, J. Long, L. Yang, W. Chen, W. Dai, X. Fu, X. Wang, Chem. Sci. 2 (2011) 1826–1830.
[28] J.H. Delcamp, A. Yella, T.W. Holcombe, M.K. Nazeeruddin, M. Grätzel, Angew. Chem. Int. Ed. 52 (2013) 376–380.
[29] X. Li, M. Wang, D. Zheng, K. Han, J. Dong, L. Sun, Energy Environ. Sci. 5 (2012) 8220–8224.
[30] T. Lazarides, T. McCormick, P. Du, G. Luo, B. Lindley, R. Eisenberg, J. Am. Chem. Soc. 131 (2009) 9192–9194.
[31] T. Sakai, D. Mersch, E. Reisner, Angew. Chem. Int. Ed. 52 (2013) 12313–12316.
[32] Z. Liang, Q. Tang, J. Liu, J. Li, F. Yan, Q. Miao, Chem. Mater. 22 (2010) 6438–6443.
[33] V.U. Pandit, S.S. Arbuj, U.P. Mulik, B.B. Kale, Environ. Sci. Technol. 48 (2014) 4178–4183.
[34] X. Zong, J. Han, B. Seger, H. Chen, G. (Max) Lu, C. Li, L. Wang, Angew. Chem. Int. Ed. 53 (2014) 4399–4403.
[35] M. Murdoch, G.I.N. Waterhouse, M.A. Nadeem, J.B. Metson, M.A. Keane, R.F. Howe, J. Llorca, H. Idriss, Nat. Chem. 3 (2011) 489–492.
[36] A.B. Laursen, S. Kegnæs, S. Dahl, I. Chorkendorff, Energy Environ. Sci. 5 (2012) 5577–5591.
[37] J.D. Benck, T.R. Hellstern, J. Kibsgaard, P. Chakthranont, T.F. Jaramillo, ACS Catal. 4 (2014) 3957–3971.
[38] Y.J. Yuan, Z.T. Yu, X.J. Liu, J.G. Cai, Z.J. Guan, Z.G. Zou, Sci. Rep. 4 (2014) 4045.
[39] M.L. Tang, D.C. Grauer, B. Lassalle-Kaiser, V.K. Yachandra, L. Amirav, J.R. Long, J. Yano, A.P. Alivisatos, Angew. Chem. Int. Ed. 50 (2011) 10203–10207.
[40] T.F. Jaramillo, K.P. Jørgensen, J. Bonde, J.H. Nielsen, S. Horch, I. Chorkendorff, Science 317 (2007) 100–102.
[41] F. Meng, J. Li, S.K. Cushing, M. Zhi, N. Wu, J. Am. Chem. Soc. 135 (2013) 10286–10289.
[42] K. Chang, Z. Mei, T. Wang, Q. Kang, S. Ouyang, J. Ye, ACS Nano. 8 (2014) 7078–7087.
[43] Y. Liu, Y.X. Yu, W.D. Zhang, J. Phys. Chem. C 117 (2013) 12949–12957.
[44] M. Shen, Z. Yan, L. Yang, P. Du, J. Zhang, B. Xiang, Chem. Commun. 50 (2014) 15447–15449.
[45] L. Ge, C. Han, X. Xiao, L. Guo, Int. J. Hydrogen Energy 38 (2013) 6960–6969.
[46] S.W. Hu, L.W. Yang, Y. Tian, X.L. Wei, J.W. Ding, J.X. Zhong, P.K. Chu, Appl. Catal. B: Environ. 163 (2015) 611–622.
[47] W. Han, C. Zang, Z. Huang, H. Zhang, L. Ren, X. Qi, J. Zhong, Int. J. Hydrogen Energy 39 (2015) 19502–19512.
[48] M.J. Frisch, G.W. Trucks, H.B. Schlegel, G.E. Scuseria, M.A. Robb, J.R. Cheeseman, G. Scalmani, V. Barone, B. Mennucci, G.A. Petersson, H. Nakatsuji, M. Caricato, X. Li, H.P. Hratchian, A.F. Izmaylov, J. Bloino, G. Zheng, J.L. Sonnenberg, M. Hada, M. Ehara, K. Toyota, R. Fukuda, J. Hasegawa, M. Ishida, T. Nakajima, Y. Honda, O. Kitao, H. Nakai, T. Vreven Jr., J.A. Montgomery, J.E. Peralta, F. Ogliaro, M. Bearpark, J.J. Heyd, E. Brothers, K.N. Kudin, V.N. Staroverov, R. Kobayashi, J. Normand, K. Raghavachari, A. Rendell, J.C. Burant, S.S. Iyengar, J. Tomasi, M. Cossi, N. Rega, J.M. Millam, M. Klene, J.E. Knox, J.B. Cross, V. Bakken, C. Adamo, J. Jaramillo, R. Gomperts, R.E. Stratmann, O. Yazyev, A.J. Austin, R. Cammi, C. Pomelli, J.W. Ochterski, R.L. Martin, K. Morokuma, V.G. Zakrzewski, G.A. Voth, P. Salvador, J.J. Dannenberg, S. Dapprich, A.D. Daniels, Ö. Farkas, J.B. Foresman, J.V. Ortiz, J. Cioslowski, D.J. Fox, Gaussian Inc., Wallingford, CT, 2009.
[49] Y. Wang, J. Zhang, X. Wang, M. Antonietti, H. Li, Angew. Chem. Int. Ed. 49 (2010) 3356–3359.
[50] P. De Marco, F. Bisti, F. Fioriti, M. Passacantando, C. Bittencourt, S. Lettieri, A. Ambrosio, P. Maddalena, S. Prezioso, S. Santucci, L. Ottaviano, J. Appl. Phys. 112 (2012) 013512.
[51] Y. Hou, A.B. Laursen, J. Zhang, G. Zhang, Y. Zhu, X. Wang, S. Dahl, I. Chorkendorff, Angew. Chem. Int. Ed. 52 (2013) 3621–3625.
[52] W. Zhou, Z. Yin, Y. Du, X. Huang, Z. Zeng, Z. Fan, H. Liu, J. Wang, H. Zhang, Small 9 (2013) 140–147.
[53] K. Maeda, X. Wang, Y. Nishihara, D. Lu, M. Antonietti, K. Domen, J. Phys. Chem. C 113 (2009) 4940–4947.
[54] F.F. Schweinberger, M.J. Berr, M. Döblinger, C. Wolff, K.E. Sanwald, A.S. Crampton, C.J. Ridge, F. Jäckel, J. Feldmann, M. Tschurl, U. Heiz, J. Am. Chem. Soc. 135 (2013) 13262–13265.
[55] Z. Hu, J. Yu, J. Mater. Chem. A 1 (2013) 12221–12228.
[56] Y. Li, H. Wang, L. Xie, Y. Liang, G. Hong, H. Dai, J. Am. Chem. Soc. 133 (2011) 7296–7299.
[57] Y. Zhu, Q. Ling, Y. Liu, H. Wang, Y. Zhu, Phys. Chem. Chem. Phys. 17 (2015) 933–940.